The Astrophysical Journal, 763:100 (10pp), 2013 February 1 doi:10.1088/0004-637X/763/2/100

IMPACT OF A REVISED ^{25}Mg$(p,\gamma)^{26}$Al REACTION RATE ON THE OPERATION OF THE Mg–Al CYCLE

O. Straniero[1,2], G. Imbriani[2,3], F. Strieder[4], D. Bemmerer[5], C. Broggini[6], A. Caciolli[6,7], P. Corvisiero[8], H. Costantini[8,9], S. Cristallo[1,2], A. DiLeva[2,3], A. Formicola[10], Z. Elekes[11], Zs. Fülöp[11], G. Gervino[12], A. Guglielmetti[13], C. Gustavino[10], Gy. Gyürky[11], M. Junker[10], A. Lemut[8,16], B. Limata[2,3], M. Marta[5,17], C. Mazzocchi[12,15], R. Menegazzo[6], L. Piersanti[1,2], P. Prati[8], V. Roca[2,3], C. Rolfs[4], C. Rossi Alvarez[6], E. Somorjai[11], F. Terrasi[2,14], and H.-P. Trautvetter[4]

[1] INAF-Osservatorio Astronomico di Collurania, Teramo, Italy; straniero@oa-teramo.inaf.it
[2] INFN Sezione di Napoli, Napoli, Italy
[3] Dipartimento di Scienze Fisiche, Università di Napoli "Federico II," Napoli, Italy
[4] Institut für Experimentalphysik, Ruhr-Universität Bochum, Bochum, Germany
[5] Helmholtz-Zentrum Dresden-Rossendorf, Bautzner Landstr. 400, Germany
[6] Istituto Nazionale di Fisica Nucleare (INFN), Sezione di Padova, via Marzolo 8, I-35131 Padova, Italy
[7] Legnaro National Laboratory (INFN), Legnaro (Padova), Italy
[8] Università di Genova and INFN Sezione di Genova, Genova, Italy
[9] CPPM, Aix-Marseilles Université, CNRS/IN2P3, Marseille, France
[10] INFN, Laboratori Nazionali del Gran Sasso (LNGS), Assergi (AQ), Italy
[11] Institute of Nuclear Research (ATOMKI), Debrecen, Hungary
[12] Dipartimento di Fisica Università di Torino and INFN Sezione di Torino, Torino, Italy
[13] Università degli Studi di Milano and INFN, Sezione di Milano, Italy
[14] Seconda Università di Napoli, Caserta, Italy
[15] University of Warsaw, 00-681 Warszawa, Poland

Received 2012 June 26; accepted 2012 November 12; published 2013 January 15

ABSTRACT

Proton captures on Mg isotopes play an important role in the Mg–Al cycle active in stellar H-burning regions. In particular, low-energy nuclear resonances in the ^{25}Mg$(p,\gamma)^{26}$Al reaction affect the production of radioactive ^{26}Al^{gs} as well as the resulting Mg/Al abundance ratio. Reliable estimations of these quantities require precise measurements of the strengths of low-energy resonances. Based on a new experimental study performed at the Laboratory for Underground Nuclear Astrophysics, we provide revised rates of the ^{25}Mg$(p,\gamma)^{26}$Al^{gs} and the ^{25}Mg$(p,\gamma)^{26}$Al^{m} reactions with corresponding uncertainties. In the temperature range 50–150 MK, the new recommended rate of ^{26}Al^{m} production is up to five times higher than previously assumed. In addition, at $T = 100$ MK, the revised total reaction rate is a factor of two higher. Note that this is the range of temperature at which the Mg–Al cycle operates in a H-burning zone. The effects of this revision are discussed. Due to the significantly larger ^{25}Mg$(p,\gamma)^{26}$Al^{m} rate, the estimated production of ^{26}Al^{gs} in H-burning regions is less efficient than previously obtained. As a result, the new rates should imply a smaller contribution from Wolf–Rayet stars to the galactic ^{26}Al budget. Similarly, we show that the asymptotic giant branch (AGB) extra-mixing scenario does not appear able to explain the most extreme values of ^{26}Al/^{27}Al, i.e., $>10^{-2}$, found in some O-rich presolar grains. Finally, the substantial increase of the total reaction rate makes the hypothesis of self-pollution by massive AGBs a more robust explanation for the Mg–Al anticorrelation observed in globular-cluster stars.

Key words: globular clusters: general – nuclear reactions, nucleosynthesis, abundances – stars: AGB and post-AGB – stars: Wolf–Rayet

1. INTRODUCTION

Many important astronomical phenomena are related to the occurrence of the Mg–Al cycle in stellar interiors. In past decades, several potential stellar sites with an active Mg–Al cycle have been identified. In particular, this cycle is active in the deepest layer of a H-burning zone provided the temperature is sufficiently large ($T > 40$ MK). Therefore, the necessary conditions are fulfilled in the core of massive main-sequence stars ($M > 30\,M_{\odot}$) as well as in the H-burning shells of red giant branch (RGB), asymptotic giant branch (AGB), and red supergiant stars. The Mg–Al cycle is also active during explosive H-burning events, such as nova-like outbursts.

In these stars the H burning is often coupled with extended mixing episodes, such as mixing powered by convection or other physical processes, e.g., rotational-induced instabilities, so that the products of the internal nucleosynthesis may appear at the stellar surface and can be directly observed. In addition, these stars undergo intense mass-loss episodes and, thus, they provide an important contribution to the pollution of the interstellar medium. The presence of radioactive ^{26}Al (ground state half-life $t_{1/2} \approx 7 \times 10^5$ yr) in different astronomical environments may be a trace of the operation of the Mg–Al cycle in stellar interiors. For example, the detection of the 1.809 MeV γ-ray line demonstrates that a few $M_{\odot}$ of this isotope are presently alive in the galactic disk (see Diehl et al. 2006). On the other hand, the excess of ^{26}Mg in the solar system material proves that some radioactive ^{26}Al has been injected into the presolar nebula shortly before the solar system formation, about 4.5 Gyr ago (Lee et al. 1977; Gallino et al. 2004). Furthermore, a ^{26}Mg excess has also been found in several presolar grains, such as SiC grains belonging to the so-called mainstream type (Zinner et al. 1991). These grains most likely condensed in atmospheres of C-rich AGB stars and, therefore, are believed to be fingerprints of the chemical composition of these stars. Finally, evidence of the operation of the Mg–Al cycle is commonly found in globular-cluster stars, which show a clear anticorrelation

[16] Current address: Lawrence Berkeley National Laboratory, Berkley, CA 94720, USA.
[17] Current address: GSI Helmholtzzentrum für Schwerionenforschung GmbH, D-64291 Darmstadt, Germany.

between Mg and Al (Kraft et al. 1997; Gratton et al. 2001). This anticorrelation is usually ascribed to an early pollution (occurring about 13 Gyr ago) of the intra-cluster gas caused by massive AGB, perhaps super-AGB, stars.[18]

An accurate understanding of the stellar sites where the Mg–Al cycle takes place may provide solutions for many open issues in stellar evolution, stellar nucleosynthesis, and chemical evolution. Spectroscopic observations of Al and Mg coupled with information about the radioactive decay of ^{26}Al derived from direct observations, e.g., γ-ray astronomy, or indirect measures, e.g., isotopic analysis of the solar system and presolar material, may constrain stellar models in a wide range of stellar masses and evolutionary phases. These correlations provide unique opportunities to study the coupling between mixing processes and nuclear burning.

However, this work requires a precise evaluation of the nuclear reaction rates of the Mg–Al cycle. As part of a long experimental campaign on H-burning reactions, the LUNA (Laboratory for Underground Nuclear Astrophysics) collaboration has recently measured the ^{25}Mg$(p,\gamma)^{26}$Al rate at the Gran Sasso National Laboratory (Strieder et al. 2012). In the present work, we use these new measurements to revise the rate of this important Mg–Al cycle reaction. In the next section, we briefly review the status of the experimental data in the relevant astrophysical energy region and recommend a set of nuclear physics parameters that should be used for the reaction rate calculations. As shown in Figure 3, the proton capture on ^{25}Mg may produce ^{26}Al in two different states, namely, the ground state and the isomeric state at $E_x = 228$ keV. The corresponding reaction rates are provided in Section 3 as a function of temperature. A final discussion follows where some of the possible astrophysical applications are addressed.

2. EXPERIMENTAL STUDIES OF THE ^{25}Mg(p,γ)^{26}Al REACTION

The astrophysical reaction rate of ^{25}Mg$(p,\gamma)^{26}$Al (Q = 6.306 MeV) is dominated by narrow resonances. These resonances have been studied in previous experiments down to a low-energy limit of $E = 189$ keV (Champagne et al. 1983a, 1983b, 1986, 1989; Endt et al. 1986, 1988; Endt & Rolfs 1987; Iliadis et al. 1990, 1996; Endt 1990; Powell et al. 1998). The known ^{26}Al level structure suggested the existence of additional low-lying resonances at $E = 37$, 57, 92, 108, and 130 keV, among which the 92 keV resonance appears most important for astrophysical temperatures from 50 to 120 MK. These low-energy resonances, indeed, were identified in indirect experiments through transfer reaction studies (see Iliadis et al. 1996, and references therein).

Recently, in an experiment at the underground 400 kV LUNA accelerator in the Laboratori Nazionali del Gran Sasso (Costantini et al. 2009; Broggini et al. 2010) the resonance at 92 keV was observed for the first time in a direct study (Strieder et al. 2012). The resonance strengths of the 92, 189, and 304 keV resonances have been measured with unprecedented sensitivity, taking full advantage of the extremely low γ-ray background level in the Gran Sasso laboratory. The Gran Sasso underground laboratory, where an average rock coverage of 1400 m (3800 m water equivalent) reduces the γ-ray background signal by several orders of magnitude (Costantini et al. 2009), is the ideal location for measurements of many astrophysically important nuclear reactions. In spite of tremendous experimental efforts in background reduction and target sample preparation as well as improvements in γ-ray detection, other low-energy resonances are still unaccessible for direct detection.

2.1. The Resonance Strengths

The strength of a resonance is defined in terms of nuclear resonance parameters:

$$\omega\gamma = \frac{2J+1}{(2j_1+1)(2j_2+1)}\frac{\Gamma_a\Gamma_b}{\Gamma} \quad (1)$$

with J, j_1, and j_2 being the spins of resonance, projectile, and target nucleus, respectively, and Γ_a, Γ_b, and Γ being the partial widths for the entrance and exit channels and the total resonance width at the resonance energy, respectively. The resonance strength for narrow resonances as in the case of ^{25}Mg$(p,\gamma)^{26}$Al can be measured directly in the thick-target yield approximation (see Rolfs & Rodney 1988, for details). Alternatively, the resonance parameters, e.g., the proton partial width Γ_p of the entrance channel, can be obtained from indirect experiments (see below).

The determination of weak low-energy resonance strengths from direct measurements is usually extremely difficult. Small target contaminations, e.g., oxygen, as well as stoichiometry changes under heavy proton bombardment may have a large effect on the absolute determination. A measurement relative to a well-known resonance can often avoid such difficulties. In Strieder et al. (2012), the low-energy resonances have been normalized to the 304 keV resonance which, in turn, was precisely measured with several different experimental techniques (Limata et al. 2010). The resonance strength values used for the present reaction rate calculation are summarized in Table 1 and compared to NACRE (Angulo et al. 1999) and a more recent compilation by Iliadis et al. (2010b). Additionally, the ground state feeding probability and the electron screening correction for directly measured $\omega\gamma$ values are listed.

2.2. Indirect Experiments

The NACRE (Angulo et al. 1999) rate at low temperatures (resonances below 130 keV) is mainly based on a reanalysis (Iliadis et al. 1996) of proton partial width values from older proton-stripping data (Betts et al. 1978; Champagne et al. 1989; Rollefson et al. 1990). The same source of information was used in Iliadis et al. (2010b).

The proton width of the 92 keV resonance calculated from the recent direct experiment, $\Gamma_p = (5.6 \pm 1.1) \times 10^{-10}$ eV (Strieder et al. 2012), deviates from the value used in the compilations, $\Gamma_p = (2.8 \pm 1.1) \times 10^{-10}$ eV (Iliadis et al. 2010a), by 1.8σ. Therefore, at the 90% confidence level the two values are incompatible, while the proton width of Strieder et al. (2012) is in good agreement with the original value of Rollefson et al. (1990), $\Gamma_p = (5.2 \pm 1.3) \times 10^{-10}$ eV. In contrast to the 92 keV resonance where a large spread of the indirect data is obvious (see Table II in Iliadis et al. 1996), the proton width data for the 37 and 57 keV resonances from different experiments are in much better agreement and we used the value quoted in Iliadis

[18] In the following, we use "massive AGB" to refer to stars with an initial mass between ~5 and ~8 $M_\odot$. After the core He burning, they form a degenerate C–O core and experience an AGB phase. We use "super-AGB" to refer to stars with an initial mass between ~8 and ~10 $M_\odot$. These stars ignite carbon in the degenerate core (usually it is an off-center ignition due to the plasma neutrino cooling), form an O–Ne core, and enter the super-AGB phase (Ritossa et al. 1996). Note that the exact values of these mass limits depend on the chemical composition and their theoretical derivation is significantly affected by the uncertainties of several types of input physics.

Table 1
The New Recommended ^{25}Mg$(p,\gamma)^{26}$Al Resonance Strengths (Uncorrected for Screening) and Corresponding Ground State Fractions f_0

E (keV)[b]	Present Work			Iliadis et al. (2010b)		Angulo et al. (1999)(NACRE)[a]
	$\omega\gamma$ (eV)	f_{es}	f_0	$\omega\gamma$ (eV)	f_0[c]	$\omega\gamma$ (eV)
37.0	$(4.5 \pm 1.8) \times 10^{-22}$[d]	...	0.79 ± 0.05[e]	$(4.5 \pm 1.8) \times 10^{-22}$	0.79	$(2.4^{+21.6}_{-2.4}) \times 10^{-21}$
57.4	$(2.8 \pm 1.1) \times 10^{-13}$[d]	...	0.81 ± 0.05[e]	$(2.8 \pm 1.1) \times 10^{-13}$	0.81	$(2.82^{+1.41}_{-0.94}) \times 10^{-13}$
92.2	$(2.9 \pm 0.6) \times 10^{-10}$[f]	1.25 ± 0.08	$0.6^{+0.2}_{-0.1}$[f]	$(1.16 \pm 0.46) \times 10^{-10}$	0.85	$(1.16^{+1.16}_{-0.39}) \times 10^{-10}$
189.5	$(9.0 \pm 0.6) \times 10^{-7}$[f]	1.08 ± 0.03	0.75 ± 0.02[f]	$(7.2 \pm 1.0) \times 10^{-7}$	0.66	$(7.1 \pm 0.9) \times 10^{-7}$
304.0	$(3.08 \pm 0.13) \times 10^{-2}$[g]	1.04 ± 0.01	0.878 ± 0.010[g]	$(3.0 \pm 0.4) \times 10^{-2}$	0.87	$(3.1 \pm 0.2) \times 10^{-2}$

Notes. The parameters for resonances not listed here were taken from Iliadis et al. (2010a). The electron screening enhancement factor f_{es} was calculated according to Assenbaum et al. (1987).
[a] The numerical values used for the ground state feeding probability are not provided.
[b] From Endt & Rolfs (1987), the uncertainty is less than 0.2 keV in all cases.
[c] From Endt & Rolfs (1987).
[d] From Iliadis et al. (2010a).
[e] From Endt & Rolfs (1987) where a larger uncertainty than originally quoted was assumed.
[f] From Strieder et al. (2012).
[g] From Limata et al. (2010).

et al. (2010a) for the present work. As a general rule we have used data from direct experiments whenever available and the results from indirect measurements were included only where no direct data exist.

2.3. The Ground State Feeding Factor

The ^{25}Mg$(p,\gamma)^{26}$Al resonances decay through complex γ-ray cascades either to the 5^+ ground state or the 0^+ isomeric state at $E_x = 228$ keV. The ground state feeding is of particular relevance for astronomy since the ^{26}Al ground state decays into the first excited state of ^{26}Mg with subsequent γ-ray emission observed by satellite telescopes. The isomeric state of ^{26}Al decays ($T_{1/2} = 6.3$ s) exclusively to the ground state of ^{26}Mg and does not lead to the emission of γ-rays. Therefore, a precise determination of the ground state feeding probability f_0 is important for the reaction rate calculation.

For the 189 and 304 keV resonances, this parameter could be reinvestigated experimentally in a high-resolution study using a high-purity germanium detector (Limata et al. 2010; Strieder et al. 2012). A high-precision determination for the low-energy resonances was impossible and the ground state feeding probabilities for these resonances rely mainly on previous literature information. The main source of information on the feeding probability is Endt & Rolfs (1987), which is to a large extent based on the experimental work published in Endt et al. (1988). For resonances at 37 and 57 keV the feeding probability seems to be well grounded while for the 92 keV resonance there is no experimental information from Endt et al. (1988). Unfortunately, the alternative literature information in the case of the 92 keV resonance is contradictory. A probability of 80% ± 15% was deduced from the experimental branching ratio determination measured in the ^{24}Mg$(^3$He$,p\gamma)^{26}$Al reaction (Champagne et al. 1983a, 1983b). However, in Champagne et al. (1986), the same authors quote a value of 61%, while the compilation of Endt & Rolfs (1987) gives 85%. The origin of this large discrepancy is unknown, but may be attributed to different assumptions on the secondary branching ratios. Recent measurements (Strieder et al. 2012) suggested a stronger feeding of ^{26}Al states that predominately decay to the isomeric state reducing the ground state fraction. Therefore, a ground state feeding probability of 60^{+20}_{-10}%, as recommended by Strieder et al. (2012), has been used in the present work for the 92 keV resonance. In general, the small uncertainty, e.g., 1%, quoted in Endt & Rolfs (1987) seems questionable due to the disagreement for certain resonances and a larger uncertainty has been assigned to these values (see Table 1).

2.4. Electron Screening in Laboratory Studies

In astrophysical environments, nuclear reactions usually take place at energies far below the Coulomb barrier where the probability for the incoming particle to overcome the repulsive force of the interacting partner decreases steeply with decreasing energy (Rolfs & Rodney 1988). In laboratory studies, the target nuclei are in most cases in the form of atoms or molecules while projectiles are usually in the form of positively charged ions. The atomic (or molecular) electron clouds surrounding the reacting nuclei act as a screening potential reducing the Coulomb barrier effectively seen by the penetrating particles. Thus, the penetration through a shielded Coulomb barrier at a given projectile energy E is equivalent to that of bare nuclei at energy $E_{\rm eff} = E + U_e$. This so-called electron screening effect (Assenbaum et al. 1987) becomes very important for large nuclear charges at low energies.

In general, a resonance strength $\omega\gamma$ is proportional to the penetration probability through the Coulomb barrier, the penetrability $P_l(E)$ of the orbital angular momentum l: $\omega\gamma \propto \Gamma_{\rm p} \propto P_l(E)$. Thus, the enhancement factor f_{es} of the entrance channel can be expressed as

$$f_{es} = \frac{\omega\gamma_{\rm screen}}{\omega\gamma_{\rm bare}} = \frac{P_l(E+U_e)}{P_l(E)}, \quad (2)$$

and for small l the approximation $f_{es} \approx \exp(\pi\eta U_e/E)$ is valid (Assenbaum et al. 1987) where η is the Sommerfeld parameter (Rolfs & Rodney 1988). The screening potential U_e is usually calculated in the approximation that the projectile velocity is much smaller than the Bohr velocity of the electrons (Shoppa et al. 1993). This approximation represents the so-called adiabatic limit where the electrons remain in the lowest energy state of the combined projectile and target system with the same quantum numbers as the original system. Consequently, the screening potential is given by the difference in atomic binding energy between the original system and the single positively charged combined system.

The atomic binding energies can be found in the literature, e.g., Huang et al. (1976). In the case of ^{25}Mg$(p,\gamma)^{26}$Al in

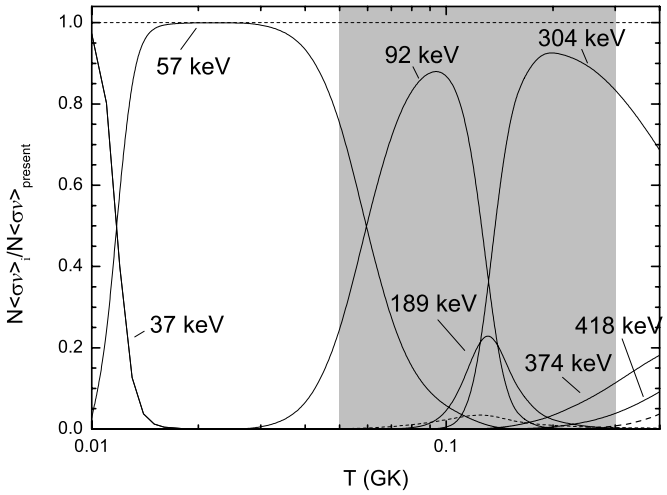

Figure 1. Ratios of individual reaction rate contributions and total recommended rate of ^{25}Mg(p, γ)^{26}Al. The dominant individual contributions are labeled while the dashed line indicates the summed contributions of weak resonances as well as resonances above $E = 420$ keV. The gray shaded area represents the temperature range for which the major revisions have been accounted in the present work.

the adiabatic limit, a value of $U_e = 1.14$ keV was calculated leading to enhancement factors f_{es} quoted in Table 1. However, in most cases, experimental investigations of the electron screening potential resulted in larger values compared to the adiabatic limit (see, e.g., Strieder et al. 2001). This discrepancy is still far from being solved and certainly deserves further studies. It is worth noting that alternative approaches have been discussed in the literature (Liolios 2001, 2003) which lead to slightly different values for the screening potential. In order to account for this ambiguity in the theoretical calculation of the electron screening potential, we assign an uncertainty to the adiabatic limit enhancement factor equal to 30% of the difference between its value and unity.

Note that the electron screening effect is already sizeable for the 304 keV resonance but has been totally neglected in previous compilations, e.g., Angulo et al. (1999) and Iliadis et al. (2010b), when low-energy resonance parameters from direct studies were used.

3. THE REACTION RATE CALCULATION

The Maxwellian-averaged two-body reaction rate can be calculated from Rolfs & Rodney (1988):

$$N_A\langle\sigma v\rangle = N_A \frac{(8/\pi)^{1/2}}{\mu^{1/2}(kT)^{3/2}} \int_0^\infty \sigma(E) E e^{-E/kT} dE, \quad (3)$$

where N_A is Avogadro's number, μ is the reduced mass, k is the Boltzmann constant, T is the temperature, $\sigma(E)$ is the cross section at the center-of-mass energy E, and v is the relative velocity of the reactants.

For narrow resonances, the reaction cross section can be expressed in the Breit–Wigner approximation and when $N_A\langle\sigma v\rangle$ is given in cm^3 mol^{-1} s^{-1}, this leads to

$$N_A\langle\sigma v\rangle = \frac{1.54 \times 10^{11}}{(\mu T_9)^{3/2}} \sum_i f_i \omega\gamma_i e^{-11.605 E_i/T_9}, \quad (4)$$

where the energy E is in MeV, μ is in amu, T_9 is the temperature in GK, and $(\omega\gamma)_i$ and f_i are the strength (in units of MeV) and ground state feeding probability of the ith resonance, respectively.

Table 2
Reaction Rate for ^{25}Mg(p, γ)^{26}Al^{gs} (cm^3 mol^{-1} s^{-1})

T (GK)	Lower Limit	Recommended Value	Upper Limit
0.010	8.23×10^{-33}	1.22×10^{-32}	1.81×10^{-32}
0.011	4.58×10^{-31}	6.37×10^{-31}	8.89×10^{-31}
0.012	2.21×10^{-29}	2.95×10^{-29}	3.95×10^{-29}
0.013	9.24×10^{-28}	1.32×10^{-27}	1.88×10^{-27}
0.014	2.87×10^{-26}	4.21×10^{-26}	6.20×10^{-26}
0.015	6.00×10^{-25}	8.90×10^{-25}	1.32×10^{-24}
0.016	8.71×10^{-24}	1.30×10^{-23}	1.93×10^{-23}
0.018	7.50×10^{-22}	1.12×10^{-21}	1.67×10^{-21}
0.020	2.61×10^{-20}	3.89×10^{-20}	5.82×10^{-20}
0.025	1.49×10^{-17}	2.21×10^{-17}	3.31×10^{-17}
0.030	9.70×10^{-16}	1.45×10^{-15}	2.16×10^{-15}
0.040	1.71×10^{-13}	2.52×10^{-13}	3.72×10^{-13}
0.050	4.28×10^{-12}	5.96×10^{-12}	8.39×10^{-12}
0.060	4.86×10^{-11}	6.25×10^{-11}	8.32×10^{-11}
0.070	3.34×10^{-10}	4.17×10^{-10}	5.62×10^{-10}
0.080	1.54×10^{-9}	1.93×10^{-9}	2.68×10^{-9}
0.090	5.28×10^{-9}	6.68×10^{-9}	9.39×10^{-9}
0.100	1.48×10^{-8}	1.87×10^{-8}	2.62×10^{-8}
0.110	3.82×10^{-8}	4.70×10^{-8}	6.39×10^{-8}
0.120	1.05×10^{-7}	1.23×10^{-7}	1.55×10^{-7}
0.130	3.53×10^{-7}	3.87×10^{-7}	4.41×10^{-7}
0.140	1.38×10^{-6}	1.45×10^{-6}	1.55×10^{-6}
0.150	5.41×10^{-6}	5.63×10^{-6}	5.87×10^{-6}
0.160	1.93×10^{-5}	2.01×10^{-5}	2.09×10^{-5}
0.180	1.75×10^{-4}	1.82×10^{-4}	1.90×10^{-4}
0.200	1.05×10^{-3}	1.09×10^{-3}	1.14×10^{-3}
0.250	2.64×10^{-2}	2.75×10^{-2}	2.86×10^{-2}
0.300	2.26×10^{-1}	2.35×10^{-1}	2.44×10^{-1}
0.350	1.05×10^{0}	1.09×10^{0}	1.13×10^{0}
0.400	3.34×10^{0}	3.46×10^{0}	3.59×10^{0}
0.450	8.29×10^{0}	8.59×10^{0}	8.89×10^{0}
0.500	1.73×10^{1}	1.79×10^{1}	1.85×10^{1}
0.600	5.28×10^{1}	5.48×10^{1}	5.67×10^{1}
0.700	1.20×10^{2}	1.24×10^{2}	1.28×10^{2}
0.800	2.23×10^{2}	2.31×10^{2}	2.40×10^{2}
0.900	3.66×10^{2}	3.79×10^{2}	3.93×10^{2}
1.000	5.40×10^{2}	5.66×10^{2}	5.95×10^{2}
1.250	1.14×10^{3}	1.19×10^{3}	1.25×10^{3}
1.500	1.89×10^{3}	1.98×10^{3}	2.07×10^{3}
1.750	2.78×10^{3}	2.91×10^{3}	3.05×10^{3}
2.000	3.77×10^{3}	3.92×10^{3}	4.10×10^{3}

The fractional reaction rate with the contributions of individual resonances is shown in Figure 1. The reaction rate in the temperature window between 50 and 300 MK is nearly entirely determined by the resonances measured in recent LUNA experiments (Limata et al. 2010; Strieder et al. 2012) with a small contribution from the 57 keV resonance at the lower edge of this window. At larger temperatures, namely $T > 300$ MK, the contribution of high-energy resonances becomes significant (see Figure 1), but this temperature range is beyond the scope of the present work.

The reaction rate uncertainty was investigated following the Monte Carlo approach of Longland et al. (2010) randomly varying the $\omega\gamma$ values entering the calculation within their experimental uncertainties. In Tables 2 and 3, the calculated reaction rates for the ground state and isomeric state are shown together with the associated lower and upper limits which are defined by the 68% confidence level of the obtained distribution.

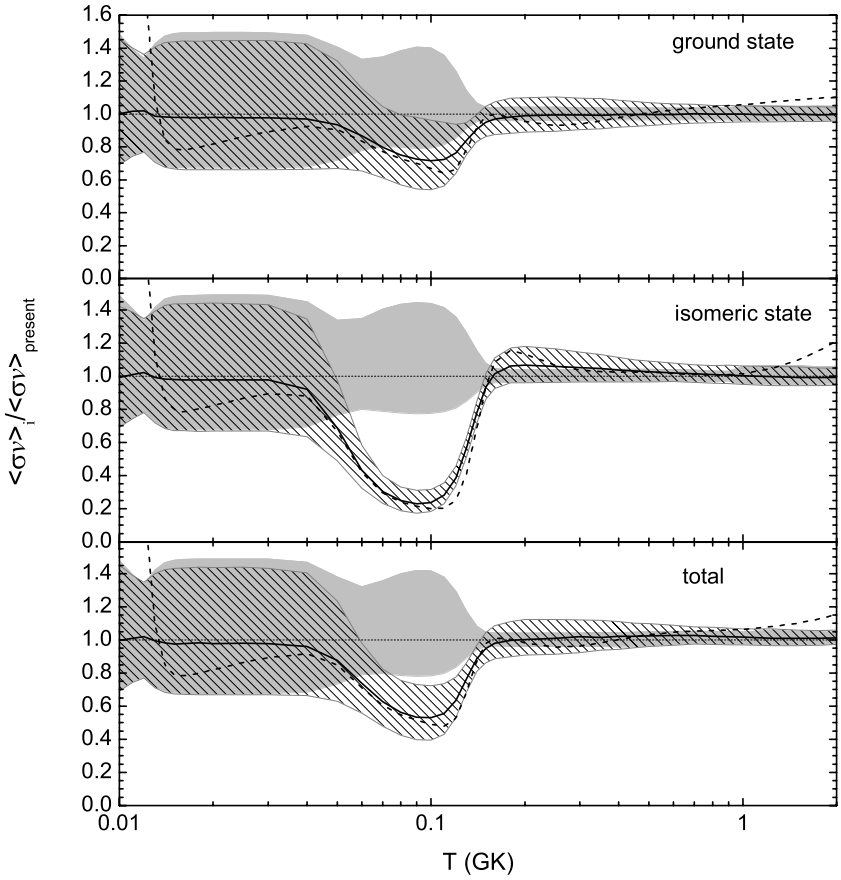

Figure 2. Comparison between the present recommended reaction rates of ^{25}Mg$(p,\gamma)^{26}$Al and those reported by NACRE (dashed lines, Angulo et al. 1999) and Iliadis et al. (2010b, solid lines). Shaded and hatched areas represent the estimated 1σ uncertainties of the present work and Iliadis et al. (2010b), respectively. Note that in Iliadis et al. (2010b) the uncertainties on the ground state feeding factors are not considered.

These new reaction rates are compared with the results of NACRE (Angulo et al. 1999) and Iliadis et al. (2010b) in Figure 2.

The present reaction rates are higher than previously found because of the higher $\omega\gamma$s recommended for the 92 and 189 keV resonances. In particular, the reaction rate for the isomeric state feeding increased by a factor of three to five for temperatures between 50 and 150 MK while the ground state reaction rate is larger by 30%–40% in the same temperature window. The larger effect on the isomeric state reaction rate arises from the revised ground state feeding probability for the 92 keV resonance (see Section 2.3 and Table 1). The uncertainty at temperatures higher than $T > 100$ MK is significantly reduced now due to the new accurate determination of the 304 keV resonance while at lower temperatures a sizeable uncertainty is still present. However, the parameters for the reaction rate calculation have been deeply revised in the present work and indirect data have been replaced by direct measurements when possible. Therefore, the present recommended reaction rates appear to be more robust than the results from previous work.

4. DISCUSSION

The new rate of the ^{25}Mg$(p,\gamma)^{26}$Al is expected to produce major effects in the temperature range $50 < T < 150$ MK. These conditions are typically found in the core of massive main-sequence stars as well as in the H-burning shell of RGB and AGB stars. In this section we review three scientific cases related to the operation of the Mg–Al cycle in these stellar environments. Our aim is to identify interesting problems of stellar evolution and nucleosynthesis whose solution requires an accurate evaluation of the ^{25}Mg$(p,\gamma)^{26}$Al rate.

To illustrate these scientific cases, we will make use of a bare nuclear network code, i.e., an appropriate set of differential equations describing the evolution of the abundances of all the isotopes of the Mg–Al cycle solved under constant temperature and density conditions. The equations are linearized and the resulting set of linear equations is solved by means of a Newton–Rhapson algorithm. The initial abundances of Mg, Al, and Si isotopes are taken from Lodders et al. (2009) and properly scaled to the adopted metallicity. To mimic the effect of an extended convective mixing, the H mass fraction is maintained as constant. The adopted nuclear network is illustrated in Figure 3.

Although a quantitative study of all the implications of the new rate would require the computation of appropriate stellar models, where the coupling of mixing and burning may be accurately accounted, a bare network calculation is adequate for most of the purposes of the present discussion. We also make use of previous results of stellar model calculations, published in the recent literature, where the effects of a change of the reaction rates have been discussed in some detail.

In the following, bare network calculations obtained by means of the new rate are compared to ones obtained by means of the rate recommended by Iliadis et al. (2010b). Note that in the quoted temperature range, the Iliadis et al. (2010b) rates for the two channels of the ^{25}Mg$(p,\gamma)^{26}$Al practically coincide with the corresponding NACRE rates.

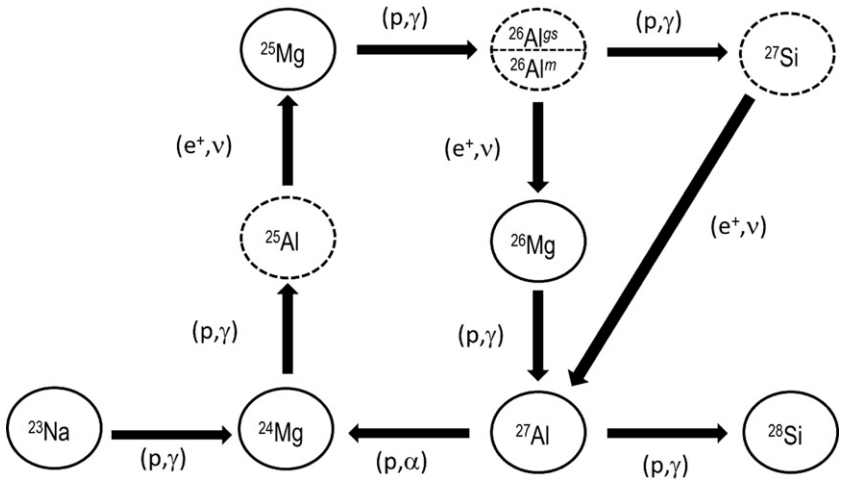

Figure 3. Mg–Al cycle: solid and dashed lines refer to stable and unstable isotopes, respectively.

Table 3
Reaction Rate for $^{25}Mg(p,\gamma)^{26}Al^m$ (cm^3 mol^{-1} s^{-1})

T (GK)	Lower Limit	Recommended Value	Upper Limit
0.010	2.31×10^{-33}	3.43×10^{-33}	5.09×10^{-33}
0.011	1.22×10^{-31}	1.72×10^{-31}	2.42×10^{-31}
0.012	5.58×10^{-30}	7.42×10^{-30}	9.89×10^{-30}
0.013	2.23×10^{-28}	3.14×10^{-28}	4.45×10^{-28}
0.014	6.79×10^{-27}	9.89×10^{-27}	1.45×10^{-26}
0.015	1.41×10^{-25}	2.08×10^{-25}	3.09×10^{-25}
0.016	2.05×10^{-24}	3.03×10^{-24}	4.50×10^{-24}
0.018	1.76×10^{-22}	2.61×10^{-22}	3.88×10^{-22}
0.020	6.14×10^{-21}	9.09×10^{-21}	1.35×10^{-20}
0.025	3.49×10^{-18}	5.16×10^{-18}	7.70×10^{-18}
0.030	2.28×10^{-16}	3.38×10^{-16}	5.03×10^{-16}
0.040	4.28×10^{-14}	6.17×10^{-14}	8.93×10^{-14}
0.050	1.41×10^{-12}	1.84×10^{-12}	2.46×10^{-12}
0.060	2.12×10^{-11}	2.66×10^{-11}	3.58×10^{-11}
0.070	1.72×10^{-10}	2.19×10^{-10}	3.07×10^{-10}
0.080	8.73×10^{-10}	1.12×10^{-9}	1.61×10^{-9}
0.090	3.14×10^{-9}	4.06×10^{-9}	5.87×10^{-9}
0.100	8.88×10^{-9}	1.15×10^{-8}	1.65×10^{-8}
0.110	2.16×10^{-8}	2.76×10^{-8}	3.90×10^{-8}
0.120	4.98×10^{-8}	6.17×10^{-8}	8.37×10^{-8}
0.130	1.21×10^{-7}	1.43×10^{-7}	1.80×10^{-7}
0.140	3.40×10^{-7}	3.77×10^{-7}	4.35×10^{-7}
0.150	1.06×10^{-6}	1.12×10^{-6}	1.21×10^{-6}
0.160	3.34×10^{-6}	3.48×10^{-6}	3.64×10^{-6}
0.180	2.74×10^{-5}	2.85×10^{-5}	2.95×10^{-5}
0.200	1.62×10^{-4}	1.68×10^{-4}	1.74×10^{-4}
0.250	4.26×10^{-3}	4.42×10^{-3}	4.59×10^{-3}
0.300	3.89×10^{-2}	4.04×10^{-2}	4.20×10^{-2}
0.350	1.93×10^{-1}	2.01×10^{-1}	2.09×10^{-1}
0.400	6.53×10^{-1}	6.81×10^{-1}	7.10×10^{-1}
0.450	1.72×10^{0}	1.79×10^{0}	1.87×10^{0}
0.500	3.79×10^{0}	3.95×10^{0}	4.12×10^{0}
0.600	1.29×10^{1}	1.34×10^{1}	1.40×10^{1}
0.700	3.21×10^{1}	3.33×10^{1}	3.45×10^{1}
0.800	6.52×10^{1}	6.74×10^{1}	6.96×10^{1}
0.900	1.15×10^{2}	1.18×10^{2}	1.22×10^{2}
1.000	1.77×10^{2}	1.87×10^{2}	1.98×10^{2}
1.250	4.17×10^{2}	4.40×10^{2}	4.68×10^{2}
1.500	7.55×10^{2}	7.94×10^{2}	8.46×10^{2}
1.750	1.17×10^{3}	1.23×10^{3}	1.30×10^{3}
2.000	1.64×10^{3}	1.73×10^{3}	1.83×10^{3}

4.1. ^{26}Al in the Wind of Wolf–Rayet Stars

Since the 1980s, the observations of the 1.809 MeV γ-ray line emitted in star-forming regions of the Milky Way have raised interesting questions about the origin of the galactic pollution of ^{26}Al (Mahoney et al. 1984; Diehl et al. 1995, 2006). Although it is commonly accepted that massive stars, i.e., those ending their life as core-collapse supernovae, are the main source of the galactic ^{26}Al, the precise nucleosynthesis scenario is still matter of debate. Favorable conditions are expected during the advanced phases of the evolution of such massive stars. In particular, a significant contribution should come from the pre-explosive as well as the explosive nucleosynthesis occurring in the C- and Ne-burning shells (Arnett & Wefel 1978; Woosley & Weaver 1980). Nevertheless, extant theoretical models show that an additional contribution may come from Wolf–Rayet (WR) stars (Dearborn & Blake 1985). In this case, the ^{26}Al is produced within the core of very massive main-sequence stars ($M > 30\,M_{\odot}$), where the temperature exceeds 50 MK. Since the main-sequence phase, these stars experience a huge mass loss. In such a way, even material located on the top of the H-convective core, which is enriched with the ashes of the Mg–Al cycle, may be ejected. The actual contribution of the WR stars to the galactic budget of ^{26}Al is rather controversial. While Palacios et al. (2005) find that these stars provide between 20% and 50% of all of the galactic ^{26}Al, Limongi & Chieffi (2006) conclude that the cumulative yield of WRs is negligible when compared to that from C- and Ne-burning shells.

Figure 4 illustrates the nucleosynthesis scenario for the core H-burning phase of a WR precursor. The burning timescales of ^{24}Mg, ^{25}Mg, and ^{26}Al^{gs} are reported as a function of the temperature and are defined as

$$\tau_i = \frac{1}{X\rho N_A \langle \sigma v \rangle_i}, \quad (5)$$

where i denotes ^{24}Mg, ^{25}Mg, and ^{26}Al^{gs} with the corresponding reaction rates for $^{24}Mg(p,\gamma)^{25}Al$, $^{25}Mg(p,\gamma)^{26}Al^{tot}$, and $^{26}Al^{gs}(p,\gamma)^{27}Si$, respectively. We have assumed a hydrogen mass fraction of $X = 0.1$ and a density of $\rho = 100$ g cm^{-3}. All the reaction rates are from the NACRE compilation except for $^{25}Mg(p,\gamma)^{26}Al$ where we have used both the present work and the Iliadis et al. (2010b) rates. The thick solid line represents

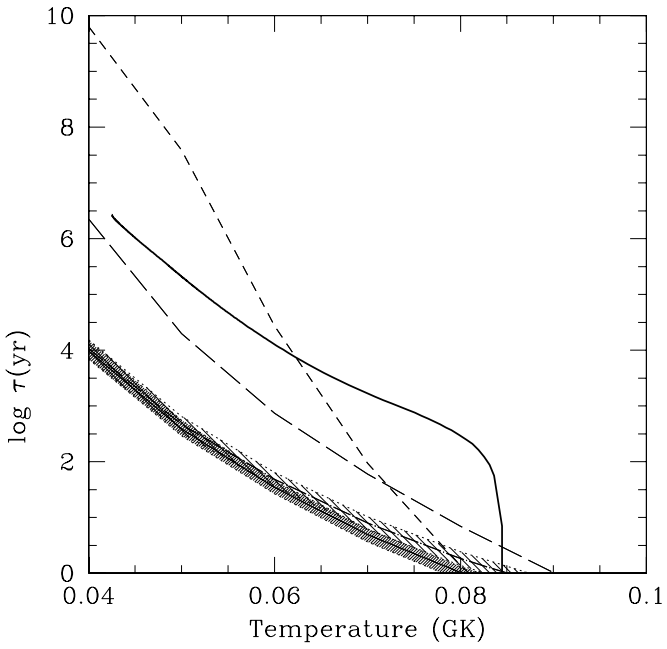

Figure 4. Burning timescales of ^{25}Mg vs. temperature, as obtained by adopting the recommended ^{25}Mg$(p,\gamma)^{26}$Al reaction rate (solid line) and the Iliadis et al. (2010b) rate (dot-dashed line). The hatched areas represent the uncertainties due to the total reaction rate. The burning timescales of ^{24}Mg and ^{26}Al^{gs} are also reported, dashed and long-dashed lines, respectively. The thick solid line represents the residual main-sequence time for 80 $M_\odot$ models (see the text for more details).

the residual time for 80 $M_\odot$ stellar models (from Limongi & Chieffi 2006), i.e., the fraction of the main-sequence lifetime during which the central temperature is larger than a given value.

During most of the main-sequence lifetime, the ^{25}Mg$(p,\gamma)^{26}$Al is the fastest process of the Mg–Al cycle. As previously found by Limongi & Chieffi (see also Iliadis et al. 2011), the corresponding ^{25}Mg-burning timescale is sufficiently short to ensure that all the ^{25}Mg available in the convective core is converted into ^{26}Al. Note that only at the end of the main sequence, when the central H is close to complete exhaustion and the temperature is about 80 MK, the burning rate of ^{24}Mg becomes as short as that of ^{25}Mg. As a result, the burning of ^{24}Mg provides a negligible contribution to the ^{25}Mg abundance in the core, and, in turn, to the ^{26}Al production. The ^{26}Al^{gs} accumulated in the convective core is marginally depleted by the subsequent proton captures because its burning timescale is about two orders of magnitude larger than that of the ^{25}Mg. Finally, since the ^{26}Al^{gs} lifetime is comparable to the stellar lifetime, its radioactive decay must be considered.

In summary, the amount of ^{26}Al accumulated in the convective core of a massive star depends, essentially, on the original ^{25}Mg content and on the branching ratio between the two output channels of the ^{25}Mg$(p,\gamma)^{26}$Al reaction. Indeed, due to the competition between ^{25}Mg$(p,\gamma)^{26}$Al^{gs} and ^{25}Mg$(p,\gamma)^{26}$Al^{m}, only a fraction of the original ^{25}Mg is actually converted into ^{26}Al^{gs}. A comparison between the previous (Iliadis et al. 2010b) and the revised branching ratios shows that at temperatures of core H-burning, the new rates imply a substantial increase of the competitive channel, i.e., the isomeric state production, than previously assumed (Figure 2). As a consequence, the ^{26}Al^{gs} production in the convective core of H-burning massive stars is less efficient than was believed. Note that this finding does not necessarily imply that the contribution of WR stars to the galactic ^{26}Al is negligible. A reliable evaluation of this contribution still resides, for example, on the poorly known mass range of these stars, which is significantly affected by mass-loss uncertainties.

4.2. Al and Mg Isotopic Composition of Presolar Grains

The chemical analysis of presolar grains, dust particles found in pristine meteorites with a size smaller than a few microns, reveals a variety of isotopic compositions. These presolar grains, e.g., mainstream SiC and O-rich grains (see Hoppe & Zinner 2000; Clayton & Nittler 2004, for a review), represent fossil records of the parent star atmospheres and provide unique information on stellar nucleosynthesis.

Mainstream SiC grains are believed to condense in the C-rich atmospheres surrounding low-mass ($M < 3\,M_\odot$) AGB stars of different metallicity ($0.001 < Z < 0.04$), which are very active nucleosynthesis sites (Iben & Renzini 1983; Busso et al. 1999; Straniero et al. 2006). Recursive dredge-up episodes powered by thermal pulses are responsible for the C enrichment of the atmosphere of these giant stars and SiC grains form when the C/O ratio becomes larger than 1, the so-called C-star phase. O-rich grains may also condense in AGB stars, but before the C-star phase is attained and C/O is still less than 1.

The ^{26}Mg excess observed in SiC as well as O-rich grains from AGB stars is interpreted as the signature of an in situ decay of ^{26}Al (Zinner et al. 1991; Nittler et al. 1994) and current theoretical models predict that low-mass AGB stars may deliver a substantial amount of ^{26}Al. The ^{26}Al is produced in the H-burning shell of an AGB star, accumulated in the H-exhausted region, and mixed via convection powered by thermal pulses to regions of higher temperatures. In the case where the maximum temperature remains below the threshold for the activation of the ^{22}Ne$(\alpha,n)^{25}$Mg reaction ($T < 300$ MK), the ^{26}Al survives and, later on, may be dredged up to the stellar surface. By contrast, the ^{26}Al is destroyed by neutron captures occurring at the bottom of the convective zone and only ^{26}Al above this zone can be dredged up (Mowlavi & Meynet 2000; Cristallo et al. 2009). Based on full network stellar model calculations, Cristallo et al. (2011) found values of ^{26}Al/^{27}Al up to 5×10^{-3}, in good agreement with those measured in mainstream SiC grains and several O-rich grains. However, in some O-rich grain values larger by up to one order of magnitude have been observed.

These extreme excesses of ^{26}Al are often explained by invoking an AGB extra-mixing which connects the bottom of the convective envelope to the hottest H-burning zone, where the Mg–Al cycle is at work. Note that the extra-mixing scenario provides a widely accepted explanation of the C and O isotopic ratios measured in the atmospheres of low-mass RGB stars (Boothroyd et al. 1994; Charbonnel 1995; Denissenkov & Weiss 1996) and O isotopic ratios found in a large sample of presolar grains suggest that extra-mixing should also be at work during the AGB phase (Nollett et al. 2003). Nevertheless, a reliable mechanism for such an extra-mixing has not yet been identified; possible candidates are rotational-induced instabilities, magnetic pipes, gravity waves, and thermohaline mixing.

The AGB extra-mixing hypothesis implies that parent stars of O-rich grains with large ^{26}Al excess never attain the C-star stage because otherwise one should also expect SiC grains showing similarly large values of ^{26}Al overabundance: this occurrence is considered a major drawback of the proposed scenario. However, as pointed out by Straniero et al. (2003), there is a lower limit for the mass of AGB stars with C/O > 1 and the larger the metallicity, the larger the minimum mass

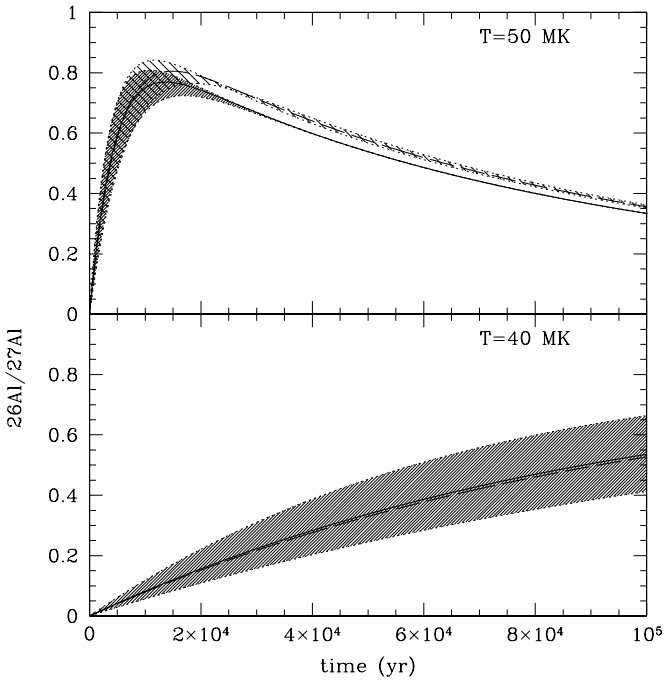

Figure 5. Evolution of the aluminum isotopic ratio for material exposed to a temperature of 40 MK (lower panel) and 50 MK (upper panel). The solid lines represent the calculation made by means of the recommended rate of the ^{25}Mg(p, γ)^{26}Al reaction, while the dashed lines have been obtained by means of the corresponding Iliadis et al. (2010b) rate. In all cases the density is 1 g cm^{-3}, $X = 0.7$. Hatched areas represent the cumulative uncertainties due to both channels of the ^{25}Mg(p, γ)^{26}Al reaction.

required, e.g., the C-star minimum mass is about 1.5 $M_\odot$ at solar metallicity, while it is only 1.3 $M_\odot$ at $Z = 0.003$. An extra-mixing in the AGB phase would increase the required minimum C-star mass because the dredged-up carbon is partially converted into nitrogen (by the CN cycle), so that the onset of the C-star stage is delayed. Thus, a very deep extra-mixing could prevent an AGB star from becoming a C-star and, at the same time, would allow for the development of high excesses of ^{26}Al.

In a recent work, Palmerini et al. (2011) showed that the O-rich grains with extreme ^{26}Mg excess can be explained by AGB stellar models with particularly deep extra-mixing, provided that (1) the initial mass is lower than 1.5 $M_\odot$ and (2) the ^{25}Mg(p, γ)^{26}Al^{gs} reaction rate is enhanced by a factor of five with respect to the Iliadis et al. (2010b) rates.

The coupling between nuclear burning and mixing makes a quantitative analysis of the impact of the new rates on the isotopic composition of O- and C-rich presolar grains difficult and would require the computation of stellar models with an extended nuclear network. This effort is beyond the purpose of the present work, but some qualitative consideration may be drawn on the basis of bare network calculations. According to Palmerini et al. (2011), the maximum temperature attained by the extra-mixing is between 40 and 50 MK, corresponding to an energy range where the ^{25}Mg proton capture rate is dominated by the 57 keV resonance (see Figure 1). In Figure 5, we report the evolution of the ^{26}Al/^{27}Al ratio for material exposed to a constant temperature of 40 MK (lower panel) and 50 MK (upper panel), respectively. In this energy range the recommended new rate for the ^{25}Mg(p, γ)^{26}Al^{gs} is only about 10% larger with respect to Iliadis et al. (2010b), while the competing channel, ^{25}Mg(p, γ)^{26}Al^{m}, is about 40% larger. As a consequence, the resulting ^{26}Al/^{27}Al isotopic ratio at $T = 50$ MK is even lower than previously found, although the total rate is larger. Moreover, in spite of the large uncertainty of the dominant 57 keV resonance contribution, we can definitely exclude an increase of a factor of five for the ^{25}Mg(p, γ)^{26}Al^{gs} rate.

In conclusion, AGB models without extra-mixing may account for ^{26}Al/^{27}Al up to 5×10^{-3}, values commonly found in mainstream SiC grains as well as in many O-rich grains from AGB stars. Larger values of ^{26}Al/^{27}Al may in part be explained by a deep extra-mixing ($T \geqslant 50$ MK), but even in the upper limit of the ^{25}Mg(p, γ)^{26}Al^{gs} rate, it is unlikely that the extra-mixing scenario could produce aluminum isotopic ratios with ^{26}Al/^{27}Al $> 10^{-2}$.

4.3. The Mg–Al Anticorrelation in Globular Cluster Stars

For many years, globular clusters (GCs) have been considered as simple stellar systems, made of nearly coeval stars and formed from a chemically homogeneous preexisting gas nebula. Nevertheless, a growing amount of photometric and spectroscopic observations indicates that many GCs actually harbor multiple stellar populations characterized by star-to-star chemical variations. Such chemical variations include the well-known O–Na and Mg–Al anticorrelations which are usually coupled to a nearly constant value of C+N+O. This chemical pattern is a characteristic signature for H burning, where the Ne–Na and the Mg–Al cycles are active. The first evidence of these "anomalies" was found in bright red giant stars (Kraft et al. 1997; Ivans et al. 1999). As it is well known, RGB stars have an extended convective envelope, but the innermost unstable layer does not reach the H-burning zone. Therefore, an extra-mixing was initially invoked to explain the observed anticorrelations. Nonetheless, this hypothesis is in contrast with the more recent discovery of O–Na and the Mg–Al anticorrelations in less evolved turnoff and sub-giant stars (Gratton et al. 2001; Yong et al. 2003). These observations definitely rule out the hypothesis that the anticorrelations are the result of an in situ physical process and prove that they were already present in the gas nebula from which these stars formed about 13 Gyr ago. Among the proposed alternative hypotheses, the pollution of the primordial gas by an early generation of massive AGB stars (perhaps super-AGB) appears promising (Cottrell & Da Costa 1981; Dantona et al. 1983; Ventura & D'Antona 2005). In these massive AGB stars, the convective envelope penetrates the regions where the H burning takes place: this phenomenon is usually called hot bottom burning (Renzini & Voli 1981). Then, the relatively low velocity wind of these stars ensures the required pollution of the intra-cluster medium. According to this scenario, stars with low Mg and high Al (or low O and high Na) would represent a second generation of cluster stars, formed after the intermediate-mass stars of the first generation passed through the AGB phase and polluted the intra-cluster gas with ashes of H burning.

However, the attempts made so far to simultaneously reproduce the observed O–Na and Mg–Al anticorrelations have produced controversial results (Fenner et al. 2004; Ventura & D'Antona 2005). Recently, Ventura et al. (2011) showed that an increase of the ^{25}Mg(p, γ)^{26}Al reaction rate by a factor of two, coupled with a more sophisticated treatment of the convective energy transport under super-adiabatic conditions, may reduce the discrepancy between the theoretical expectations and the observed cluster abundances of Mg and Al.

In order to illustrate the influence of the newly recommended reaction rates on the Mg–Al cycle operating in the H-burning shell of a massive AGB star, we have performed some bare network calculations. Values for the metallicity, the H mass fraction, the temperature, and the density representative of

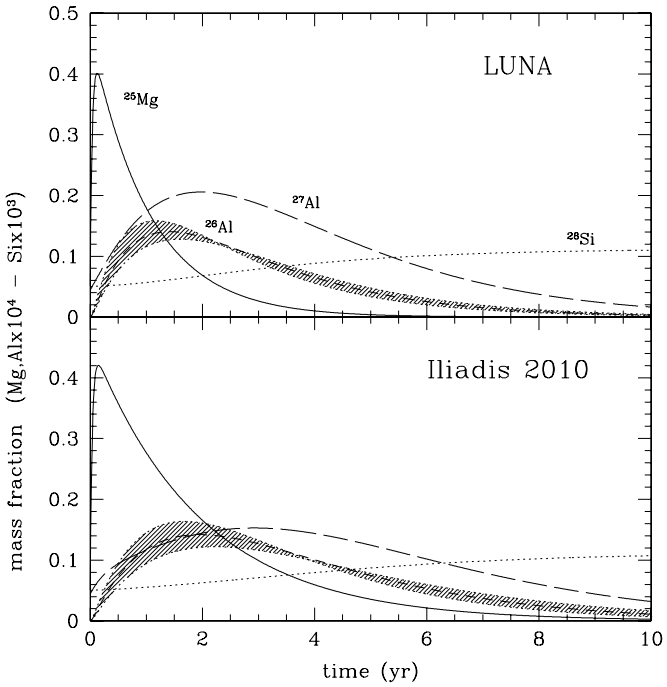

Figure 6. Evolution of Mg and Al isotopes. Temperature and density are maintained constant, namely, $T = 100$ MK and $\rho = 10$ g cm^{-3}, respectively. At $t = 0$, the composition is scaled solar and $Z = 0.001$. The H mass fraction is $X = 0.6$. The various lines represent the following isotopes: ^{25}Mg (solid), ^{26}Al (dashed), ^{27}Al (long dashed), and ^{28}Si (dotted). The calculation shown in the upper panel has been obtained by using the recommended rates of the ^{25}Mg$(p, \gamma)^{26}$Al reactions. The hatched area represents the cumulative uncertainty on the ^{26}Al^{gs} abundance due to both channels of the ^{25}Mg$(p, \gamma)^{26}$Al. For comparison, the results obtained by means of the Iliadis et al. (2010b) rates are shown in the lower panel.

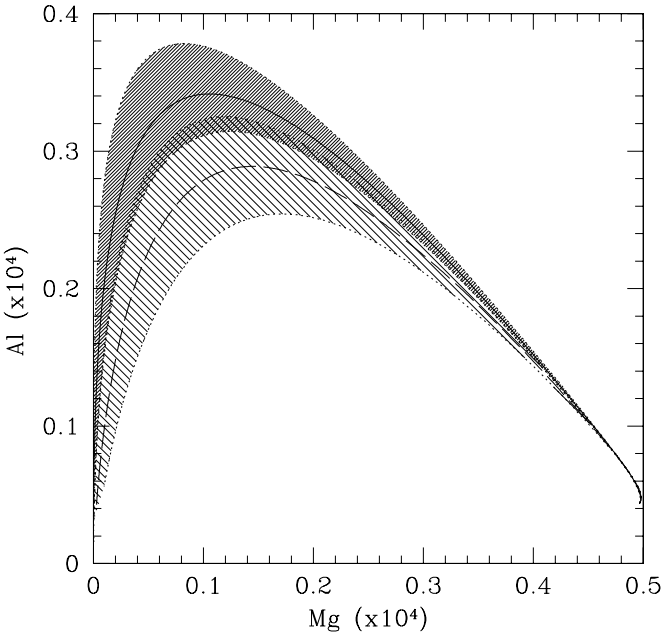

Figure 7. Al abundance vs. Mg abundance for the same case shown in Figure 6. The solid and the dashed lines refer to the calculations made by means of the new (recommended) and the Iliadis et al. (2010b) rates of the ^{25}Mg$(p, \gamma)^{26}$Al reactions, respectively. The hatched areas represent the uncertainties due to the total reaction rate.

the innermost layers of the convective envelope of a massive AGB star have been selected, namely, $Z = 0.001$, $X = 0.6$, $T = 100$ MK, and $\rho = 10$ g cm^{-3}. The result is shown in Figure 6, where the upper panel refers to the calculation obtained by means of the new reaction rates for the ^{25}Mg$(p, \gamma)^{26}$Al, while the bottom panel corresponds to the calculations obtained by adopting the Iliadis et al. (2010b) rates. The NACRE compilation has been used for all of the other reactions of the Mg–Al cycle, while for the ^{26}Al^{gs} decay rate we have assumed the terrestrial value ($\lambda = 2.97 \times 10^{-14}$ s^{-1}). The increase of the new total ^{25}Mg$(p, \gamma)^{26}$Al reaction rate by a factor of two with respect to Iliadis et al. (2010b) is indeed very close to the value found by Ventura et al. (2011) and supports the massive AGB self-pollution scenario. It should be noted that the largest variations in the evolution of the Mg and Al isotopic abundances are caused by the larger ^{25}Mg$(p, \gamma)^{26}$Al^m rate. This variation favors a prompt destruction of ^{25}Mg and a fast increase of the ^{27}Al production. In Figure 7, the Al (elemental) abundance is compared with the corresponding Mg abundance, for the $T = 100$ MK calculations. The new rate implies a steeper anticorrelation and a significant increase of the maximum Al abundance. Note the similarity of this figure to Figure 4 of Ventura et al. (2011) based on the result of AGB stellar models obtained under different assumptions for the ^{25}Mg$(p, \gamma)^{26}$Al rate.

5. SUMMARY AND CONCLUSIONS

The ^{25}Mg$(p, \gamma)^{26}$Al reaction rate has been revised on the basis of new measurements of the key resonances at $E = 92$, 189, and 304 keV. Particular efforts have been devoted to reviewing all experimental parameters, e.g., resonance strengths, ground state branching ratio fractions, and electron screening, in order to reduce the systematic uncertainty of this reaction rate in the temperature range present in stellar H-burning zones. Note that in previous works the input parameter uncertainties were partly underestimated, e.g., present uncertainties on ground state branching ratio and electron screening were not considered.

We have found a significant variation of the rate for temperature $50 < T < 150$ MK with respect to previous studies. The revised total reaction rate is about a factor of two larger than suggested by NACRE and Iliadis et al. (2010b), while the production rate of the isomeric state, which decays almost instantly into ^{26}Mg, is up to a factor of five larger. As a result, the expected production of ^{26}Al^{gs} in stellar H-burning zones is lower than previously estimated. This implies, in particular, a reduction of the estimated contribution of WR stars to the galactic production of ^{26}Al. We have also investigated the possible effect on the Mg and Al isotopic composition of presolar grains originating in AGB stars. The most important conclusion is that the deep AGB extra-mixing, often invoked to explain the large excess of ^{26}Al in some O-rich grains, does not appear a suitable solution for ^{26}Al/^{27}Al $> 10^{-2}$.

On the other hand, the substantial increase of the total reaction rate makes the globular cluster self-pollution caused by massive AGB stars a more reliable scenario for the reproduction of the Mg–Al anticorrelation.

In summary, we have demonstrated that a considerable improvement of our knowledge of the nuclear reaction rates involved in the Mg–Al cycle allows us to constrain nucleosynthesis and stellar evolution models as well as the interplay between nuclear burning and mixing processes operating simultaneously in stellar interiors. In this context, further experimental studies are required to improve the analysis reported in Section 4 and to derive more firm conclusions on the operation of the Mg–Al cycle in stellar interiors. Some input parameters still carry a significant uncertainty, e.g., the ground state branching

ratio of each nuclear resonance. Partially, as in the case of the 92 keV resonance, these branching ratios are based on experiments with rather low statistics and, therefore, we recommend a reinvestigation of these parameters in a dedicated experiment. In addition, other key reactions of the Mg–Al cycle, such as ^{24}Mg$(p,\gamma)^{25}$Al, deserve more attention. Note that ^{24}Mg is the most abundant isotope among those involved in the Mg–Al cycle and at $T > 80$ MK this reaction is faster than ^{25}Mg$(p,\gamma)^{26}$Al, thus providing additional fuel for Al production. The rate tabulated by NACRE is essentially based on the experimental result by Trautvetter & Rolfs (1975). At low energy, the cross section is dominated by a resonance at 214 keV. An experiment performed by the TUNL group (Powell et al. 1999) resulted in a 25% higher resonance strength than recommended by NACRE. Note that this result has been incorporated by Iliadis et al. (2010b) in their revised reaction rate. However, Limata et al. (2010) derive a value for the strength of the 214 KeV resonance that agrees with the older result from Trautvetter & Rolfs (1975). Further studies are required to disentangle these controversial results. Concerning the production of ^{26}Al^{gs}, a key role is played by the ^{26}Al$^{gs}(p,\gamma)^{27}$Si reaction. The only available direct measurement has been discussed in Vogelaar et al. (1996). Recently, the 184 keV resonance has been measured at TRIUMF with the recoil mass separator (Ruiz et al. 2006). An up-to-date analysis of the reaction rate has been presented by Iliadis et al. (2010b). The difficulties of these measurements are related to the radioactivity of ^{26}Al^{gs}. Also in this case further experimental investigations are mandatory.

The present work has been supported by INFN and in part by the EU (ILIAS-TA RII3-CT-2004-506222), OTKA (K101328), and DFG (Ro 429/41). We are grateful to M. Limongi for the enlightening discussions on the ^{26}Al production in massive stars. A. Di Leva, G. Imbriani, L. Piersanti, and S. Cristallo acknowledge the support of the Italian Ministry of Education, University, and Research under the FIRB2008 program. O. Straniero, L. Piersanti, and S. Cristallo have been supported by INAF under the PRIN2010 program. A. Caciolli acknowledges financial support by Fondazione Cassa Di Risparmio di Padova e Rovigo.

REFERENCES

Angulo, C., Arnould, M., Rayet, M., et al. 1999, NuPhA, 656, 3
Arnett, W. D., & Wefel, J. P. 1978, ApJL, 224, L139
Assenbaum, H., Langanke, K., & Rolfs, C. 1987, ZPhyA, 327, 461
Betts, R. R., Fortune, H. T., & Pullen, D. J. 1978, NuPhA, 299, 412
Boothroyd, A. I., Sackmann, I.-J., & Wasserburg, G. J. 1994, ApJL, 430, L77
Broggini, C., Bemmerer, D., Guglielmetti, A., & Menegazzo, R. 2010, ARNPS, 60, 53
Busso, M., Gallino, R., & Wasserburg, G. J. 1999, ARA&A, 37, 239
Champagne, A. E., Howard, A. J., Smith, M. S., Magnus, P. V., & Parker, P. D. 1989, NuPhA, 505, 384
Champagne, A. E., Howard, A. J., & Parker, P. D. 1983a, NuPhA, 402, 159
Champagne, A. E., Howard, A. J., & Parker, P. D. 1983b, NuPhA, 402, 179
Champagne, A. E., McDonald, A. B., Wang, T. F., et al. 1986, NuPhA, 451, 498
Charbonnel, C. 1995, ApJL, 453, L41
Clayton, D. D., & Nittler, L. R. 2004, ARA&A, 42, 39
Costantini, H., Formicola, A., Imbriani, G., et al. 2009, RPPh, 72, 086301
Cottrell, P. L., & Da Costa, G. S. 1981, ApJL, 245, L79
Cristallo, S., Piersanti, L., Straniero, O., et al. 2011, ApJS, 197, 17
Cristallo, S., Straniero, O., Gallino, R., et al. 2009, ApJ, 696, 797
Dantona, F., Gratton, R., & Chieffi, A. 1983, MmSAI, 54, 173
Dearborn, D. S. P., & Blake, J. B. 1985, ApJL, 288, L21
Denissenkov, P. A., & Weiss, A. 1996, A&A, 308, 773
Diehl, R., Dupraz, C., Bennett, K., et al. 1995, A&A, 298, 445
Diehl, R., Halloin, H., Kretschmer, K., et al. 2006, Natur, 439, 45
Endt, P. M. 1990, NuPhA, 521, 1
Endt, P. M., de Wit, P., & Alderliesten, C. 1986, NuPhA, 459, 61
Endt, P. M., de Wit, P., & Alderliesten, C. 1988, NuPhA, 476, 333
Endt, P. M., & Rolfs, C. 1987, NuPhA, 467, 261
Fenner, Y., Campbell, S., Karakas, A. I., Lattanzio, J. C., & Gibson, B. K. 2004, MNRAS, 353, 789
Gallino, R., Busso, M., Wasserburg, G. J., & Straniero, O. 2004, NewAR, 48, 133
Gratton, R. G., Bonifacio, P., Bragaglia, A., et al. 2001, A&A, 369, 87
Hoppe, P., & Zinner, E. 2000, JGR, 105, 10371
Huang, K.-N., Aoyagi, M., Chen, M. H., Crasemann, B., & Mark, H. 1976, ADNDT, 18, 243
Iben, I., Jr., & Renzini, A. 1983, ARA&A, 21, 271
Iliadis, C., Buchmann, L., Endt, P. M., Herndl, H., & Wiescher, M. 1996, PhRvC, 53, 475
Iliadis, C., Champagne, A., Chieffi, A., & Limongi, M. 2011, ApJS, 193, 16
Iliadis, C., Longland, R., Champagne, A. E., & Coc, A. 2010a, NuPhA, 841, 251
Iliadis, C., Longland, R., Champagne, A. E., Coc, A., & Fitzgerald, R. 2010b, NuPhA, 841, 31
Iliadis, C., Schange, T., Rolfs, C., et al. 1990, NuPhA, 512, 509
Ivans, I. I., Sneden, C., Kraft, R. P., et al. 1999, AJ, 118, 1273
Kraft, R. P., Sneden, C., Smith, G. H., et al. 1997, AJ, 113, 279
Lee, T., Papanastassiou, D. A., & Wasserburg, G. J. 1977, ApJL, 211, L107
Limata, B., Strieder, F., Formicola, A., et al. 2010, PhRvC, 82, 015801
Limongi, M., & Chieffi, A. 2006, ApJ, 647, 483
Liolios, T. E. 2001, NuPhA, 693, 847
Liolios, T. E. 2003, JPhG, 29, 1423
Lodders, K., Palme, H., & Gail, H.-P. 2009, in Abundances of the Elements in the Solar System, ed. J. E. Trümper (Berlin: Springer-Verlag), 560
Longland, R., Iliadis, C., Champagne, A. E., et al. 2010, NuPhA, 841, 1
Mahoney, W. A., Ling, J. C., Wheaton, W. A., & Jacobson, A. S. 1984, ApJ, 286, 578
Mowlavi, N., & Meynet, G. 2000, A&A, 361, 959
Nittler, L. R., O'D Alexander, C. M., Gao, X., Walker, R. M., & Zinner, E. K. 1994, Natur, 370, 443
Nollett, K. M., Busso, M., & Wasserburg, G. J. 2003, ApJ, 582, 1036
Palacios, A., Meynet, G., Vuissoz, C., et al. 2005, A&A, 429, 613
Palmerini, S., La Cognata, M., Cristallo, S., & Busso, M. 2011, ApJ, 729, 3
Powell, D. C., Iliadis, C., Champagne, A. E., et al. 1998, NuPhA, 644, 263
Powell, D. C., Iliadis, C., Champagne, A. E., et al. 1999, NuPhA, 660, 349
Renzini, A., & Voli, M. 1981, A&A, 94, 175
Ritossa, C., Garcia-Berro, E., & Iben, I., Jr. 1996, ApJ, 460, 489
Rolfs, C., & Rodney, W. S. 1988, Cauldrons in the Cosmos (Chicago, IL: Univ. of Chicago Press)
Rollefson, A. A., Wijekumar, V., Browne, C. P., et al. 1990, NuPhA, 507, 413
Ruiz, C., Parikh, A., José, J., et al. 2006, PhRvL, 96, 252501
Shoppa, T. D., Koonin, S. E., Langanke, K., & Seki, R. 1993, PhRvC, 48, 837
Straniero, O., Domínguez, I., Cristallo, S., & Gallino, R. 2003, PASA, 20, 389
Straniero, O., Gallino, R., & Cristallo, S. 2006, NuPhA, 777, 311
Strieder, F., Limata, B., Formicola, A., et al. 2012, PhLB, 707, 60
Strieder, F., Rolfs, C., Spitaleri, C., & Corvisiero, P. 2001, NW, 88, 461
Trautvetter, H. P., & Rolfs, C. 1975, NuPhA, 242, 519
Ventura, P., Carini, R., & D'Antona, F. 2011, MNRAS, 415, 3865
Ventura, P., & D'Antona, F. 2005, ApJL, 635, L149
Vogelaar, R. B., Mitchell, L. W., Kavanagh, R. W., et al. 1996, PhRvC, 53, 1945
Woosley, S. E., & Weaver, T. A. 1980, ApJ, 238, 1017
Yong, D., Grundahl, F., Lambert, D. L., Nissen, P. E., & Shetrone, M. D. 2003, A&A, 402, 985
Zinner, E., Amari, S., Anders, E., & Lewis, R. 1991, Natur, 349, 51